Identification of Piezoelectric Material Parameters [1]

Barbara Kaltenbacher, SFB F013, Johannes Kepler University Linz, Austria
Manfred Kaltenbacher, Institute of Sensor Technology, Friedrich Alexander University Erlangen-Nuremberg, Germany

Abstract. For the exact reconstruction of piezoelectric material parameters from impedance (and possibly mechanical) measurements, we propose a new iterative scheme based on finite element simulations of the full piezoelectric equations, combined with a Newton-conjugate gradient inversion scheme. Numerical experiments for a thickness resonator show that this method is able to remove undesirable inaccuraccies occurring in conventional simplified model parameter estimation techniques.

Key words. piezoelectric effect, parameter identification

1 Introduction

Piezoelectric materials are widely used in electromechanical sensors and actuators, e.g., ultrasound transducers in medical imaging and therapy, force and acceleration sensors, positioning sensors, SAW sensors, with a permanently growing range of applications. Their mode of action is based on the piezoelectric effect, that couples the electrical and the mechanical behavior of such materials. For the optimal design of piezoelectric devices, efficient numerical simulation tools have been developed, that avoid expensive and time-consuming experiments by numerically solving the mathematical formulation of the underlying physical model, i.e., a system of partial differential equations with appropriate boundary conditions (cf., e.g. [5], [4], [7]). These equations contain as essential information a set of about ten material parameters steering the interplay of mechanical and electrical quantities. A priori knowledge on the exact values of these parameters is for obvious reasons indispensable for obtaining useful results in computational system simulations. So far, these quantities have been estimated by experiments with test samples, whose special shape was supposed to allow for simplifications in the model and hence explicit formulas for their computation from the resonance frequencies (cf., e.g., [12]). However, the results of these estimation formulas do not seem to provide sufficiently precise information on the material coefficients (cf. [8]), showing deviations of up to 10-20 per cent, which gave rise to inaccurate results in the computational simulations. Moreover, the handling of such test samples is complicated and their production costly. Therefore it was our aim to propose and implement a computational scheme that enables a precise and automatic reconstruction of the whole material parameter set from relatively simple measurements, by iterative adjustment based on simulations of the full two or three dimensional piezoelectric equations.

[1]Supported by the Fonds zur Förderung der wissenschaftlichen Forschung under grant 10866 and the SFB F013/08

2 The forward problem

2.1 The Piezoelectric equations

The material law describing the piezoelectric effect in the linearized case of small mechanical deformations and electric fields, reads as

$$\vec{\sigma} = \mathbf{c}^E \vec{S} - \mathbf{e}^T \vec{E} \tag{1}$$

$$\vec{D} = \mathbf{e}\vec{S} + \varepsilon^S \vec{E} , \tag{2}$$

relating the mechanical stress $\vec{\sigma} = (\sigma_{xx}, \sigma_{yy}, \sigma_{zz}, \sigma_{xy}, \sigma_{yz}, \sigma_{xz})^T$ and the electrical displacement $\vec{D} = (D_x, D_y, D_z)^T$, respectively, to the mechanical strain $\vec{S} = (S_{xx}, S_{yy}, S_{zz}, S_{xy}, S_{yz}, S_{xz})^T$ and the electric field $\vec{E} = (E_x, E_y, E_z)$. We can rewrite $-\vec{E}$ as the gradient of a electric potential ϕ

$$\vec{E} = -\mathrm{grad}\phi ,$$

and $\vec{S}$ in terms of the mechanical displacements $\vec{d} = (d_x, d_y, d_z)$

$$\vec{S} = \mathcal{B}\vec{d} ,$$

where the first order differential operator $\mathcal{B}$ is

$$\mathcal{B} = \begin{pmatrix} \frac{\partial}{\partial x} & 0 & 0 \\ 0 & \frac{\partial}{\partial y} & 0 \\ 0 & 0 & \frac{\partial}{\partial z} \\ \frac{\partial}{\partial y} & \frac{\partial}{\partial x} & 0 \\ 0 & \frac{\partial}{\partial z} & \frac{\partial}{\partial y} \\ \frac{\partial}{\partial z} & 0 & \frac{\partial}{\partial x} \end{pmatrix} ,$$

i.e., the transposed of the divergence DIV of a dyadic. The material tensors $\mathbf{c}^E$, ε^S, and $\mathbf{e}$, appearing in (1) are the elasticity coefficients, the dielectric constants, and the piezoelectric coupling coefficients, respectively. Due to the crystal structure and the polarization of the piezoelectric material, these matrices show a certain symmetry and sparsity pattern (cf. [4]). E.g., in the 6mm crystal class, which we will concentrate on in the further expositions, this is given by

$$\mathbf{c}^E = \begin{pmatrix} c_{11}^E & c_{12}^E & c_{13}^E & 0 & 0 & 0 \\ c_{12}^E & c_{11}^E & c_{13}^E & 0 & 0 & 0 \\ c_{13}^E & c_{13}^E & c_{33}^E & 0 & 0 & 0 \\ 0 & 0 & 0 & \frac{1}{2}(c_{11}^E - c_{12}^E) & 0 & 0 \\ 0 & 0 & 0 & 0 & c_{44}^E & 0 \\ 0 & 0 & 0 & 0 & 0 & c_{44}^E \end{pmatrix}$$

$$\mathbf{e} = \begin{pmatrix} 0 & 0 & 0 & 0 & 0 & e_{15} \\ 0 & 0 & 0 & 0 & e_{15} & 0 \\ e_{31} & e_{31} & e_{33} & 0 & 0 & 0 \end{pmatrix} ,$$

$$\varepsilon^S = \begin{pmatrix} \varepsilon_{11}^S & 0 & 0 \\ 0 & \varepsilon_{11}^S & 0 \\ 0 & 0 & \varepsilon_{33}^S \end{pmatrix} \ ;$$

note however, that our approach will of course be directly applicable to material tensors of any type.

Now, by Newton's law for the mechanical behavior

$$\mathrm{DIV}\vec{\sigma} = \rho \frac{\partial^2 \vec{d}}{\partial t^2} \ ,$$

where ρ is the density, and Maxwell's equation, together with the fact that piezoelectric materials are insulating, i.e., do not contain free volume charges

$$\mathrm{div}\vec{D} = 0 \ ,$$

we arrive at a system of four partial differential equations for $\vec{d}$ and ϕ, inside a piezoelectric body Ω

$$\begin{array}{rcll} \rho\frac{\partial^2 \vec{d}}{\partial t^2} - \mathcal{B}^T\left(\mathbf{c}^E \mathcal{B}\vec{d} + \mathbf{e}^T \mathrm{grad}\phi\right) & = & 0 & \text{in } \Omega \\ -\mathrm{div}\left(\mathbf{e}\mathcal{B}\vec{d} - \varepsilon^S \mathrm{grad}\phi\right) & = & 0 & \text{in } \Omega \ . \end{array} \tag{3}$$

Considering the experimental setting of vanishing normal stress at the boundary, and two electrodes being applied at opposite positions Γ_g and Γ_e, one of them loaded with a prescribed surface charge q^e, we arrive at the boundary conditions

$$\begin{array}{rcll} \mathbf{N}^T\sigma & = & 0 & \text{on } \partial\Omega \\ \phi & = & 0 & \text{on } \Gamma_g \\ \vec{D}\cdot\vec{n} & = & -\frac{q^e}{A} & \text{on } \Gamma_e \\ \vec{D}\cdot\vec{n} & = & 0 & \text{on } \partial\Omega \setminus (\Gamma_g \cup \Gamma_e) \ , \end{array} \tag{4}$$

where

$$\mathbf{N} = \begin{pmatrix} n_x & 0 & 0 \\ 0 & n_y & 0 \\ 0 & 0 & n_z \\ n_y & n_x & 0 \\ 0 & n_z & n_y \\ n_z & 0 & n_x \end{pmatrix} \ ,$$

and A is the surface area covered by the loaded electrode. Note that electrodes are equipotential surfaces, i.e., the value of the ϕ part of a solution to (3) will be the same on all of Γ_e.

2.2 Well-posedness

A weak formulation of this boundary value problem can be obtained by testing the first line in (3) with vector-valued C^∞-functions $\vec{b} = (b_x, b_y, b_z) : \Omega \to \mathbb{R}^3$, and the second one with scalar C^∞-functions vanishing at the grounded electrode Γ_g and being constant over the loaded electrode Γ_e. Integrating by parts

$$\int_\Omega (\mathcal{B}^T\vec{\sigma})^T\vec{b}\ d\Omega = -\int_\Omega \vec{\sigma}\cdot\mathcal{B}\vec{b}\ d\Omega + \int_{\partial\Omega}(\mathbf{N}^T\vec{\sigma})^T\vec{b}\ d\Gamma\ , \tag{5}$$

and taking into account

$$\mathcal{B}^T = \mathrm{DIV}\ ,$$

we arrive at

$$\begin{aligned}
&\forall\vec{b}\in H^1_{\mathcal{B}}(\Omega)\quad w\in H^1_g(\Omega)\ :\\
&\textstyle\int_\Omega\Big(\rho(\frac{\partial^2\vec{d}}{\partial t^2})^T\vec{b} + \ (\mathcal{B}\vec{d})^T\mathbf{c}^E(\mathcal{B}\vec{b}) \quad + \quad (\mathrm{grad}\phi)^T\mathbf{e}(\mathcal{B}\vec{b}) + (\mathrm{grad}w)^T\mathbf{e}(\mathcal{B}\vec{d})\\
&\qquad\qquad\qquad\qquad\qquad\quad - \quad (\mathrm{grad}\phi)^T\varepsilon^S(\mathrm{grad}w)\Big)\ d\Omega = -q^e w|_{\Gamma_e}\ .
\end{aligned} \tag{6}$$

The function spaces

$$H^1_g := \overline{\{w\in C^\infty(\Omega)\ :\ w|_{\Gamma_g}=0\wedge\exists c\in\mathbb{R}: w|_{\Gamma_e}\equiv c\}}^{H^1}\ ,$$

$$H^1_{\mathcal{B}} := \overline{(C^\infty(\Omega))^3}^{H^1_{\mathcal{B}}}\ ,\quad ||\vec{b}||_{H^1_{\mathcal{B}}} := ||\vec{b}||_{L^2} + ||\mathcal{B}\vec{b}||_{L^2}\ ,$$

are the closures of the above mentioned test function spaces with respect to in this context reasonable topologies. Taking Fourier transforms in time $\hat{\vec{d}}$ of $\vec{d}$, and $\hat{\phi}$ of ϕ, we arrive at the frequency domain formulation

$$\begin{aligned}
&\forall\vec{b}\in H^1_{\mathcal{B}\ \mathbb{C}}(\Omega)\quad w\in H^1_{g\ \mathbb{C}}(\Omega)\ :\\
&\textstyle\int_\Omega\Big(-\rho\omega^2\hat{\vec{d}}^T\vec{b} \ + \ (\mathcal{B}\hat{\vec{d}})^T\mathbf{c}^E(\mathcal{B}\vec{b}) \quad + \quad (\mathrm{grad}\hat{\phi})^T\mathbf{e}(\mathcal{B}\vec{b}) + (\mathrm{grad}w)^T\mathbf{e}(\mathcal{B}\hat{\vec{d}})\\
&\qquad\qquad\qquad\qquad\qquad\quad - \quad (\mathrm{grad}\hat{\phi})^T\varepsilon^S(\mathrm{grad}w)\Big)\ d\Omega = -\hat{q}^e w|_{\Gamma_e}
\end{aligned} \tag{7}$$

which, since $\rho,\omega,\mathbf{c}^E,\mathbf{e}$, and ε^S are real-valued, can be considered separately for the real and imaginary parts of $\hat{\vec{d}}$, $\hat{\phi}$.

Regarding (7) for fixed frequency ω as a weak differential equation with respect to the space variables, one immediately obtains some assertions on its well-posedness by using well-known results on eigenvalues of coercive operators. We consider the slightly simplified but realistic situation of parallel electrodes covering, e.g., the top $x=L$ and bottom $x=0$ of the piezoelectric sample $\Omega=(0,L)\times\tilde{\Omega}$. Then it follows from

$$\begin{aligned}
\textstyle\int_\Omega(\mathrm{grad}w)^T\varepsilon^S(\mathrm{grad}w)\Big)\ d\Omega \ &\geq\ \lambda_{\min}(\varepsilon^S)\,\|\mathrm{grad}w\|^2_{L^2}\\
&\geq\ \tfrac{\lambda_{\min}(\varepsilon^S)}{(2L\,\|w\|_{L^2})^2}\Big(-\textstyle\int_0^L\int_{\tilde{\Omega}}2x\cdot w\frac{\partial w}{\partial x}\ d\tilde{\Omega}\ dx\Big)^2\\
&=\ \tfrac{\lambda_{\min}(\varepsilon^S)}{(2L\,\|w\|_{L^2})^2}\Big(\textstyle\int_0^L\int_{\tilde{\Omega}}w^2\ d\tilde{\Omega}\ dx\Big)^2 = \tfrac{\lambda_{\min}(\varepsilon^S)}{(2L)^2}\,\|w\|_{L^2}\ ,
\end{aligned}$$

for $w \in H_g^1$, where we have used simple integration by parts in the x-direction, that the part of (7) belonging to the second line in (3) (i.e., setting $\vec{b} \equiv 0$ in (7)) induces an elliptic equation that therefore can be resolved (in the weak sense) with respect to $\hat{\phi}$:

$$\begin{aligned} \Re(\hat{\phi}(\omega)) &= (-\triangle_\epsilon)^{-1}\Big(- \triangle_{\mathbf{e}}\, \Re(\vec{\hat{d}}(\omega)) + \Re(\hat{q}^e(\omega))\delta_{\Gamma_e}\Big) \\ \Im(\hat{\phi}(\omega)) &= (-\triangle_\epsilon)^{-1}\Big(- \triangle_{\mathbf{e}}\, \Im(\vec{\hat{d}}(\omega)) + \Im(\hat{q}^e(\omega))\delta_{\Gamma_e}\Big). \end{aligned} \tag{8}$$

Here

$$\begin{array}{rcl} -\triangle_\epsilon \;:\; H_g^1 & \to & (H_g^1)^* \\ w & \mapsto & \left\{ \begin{array}{rcl} -\triangle_\epsilon\, w \;:\; H_g^1 & \to & \mathbb{R} \\ v & \mapsto & \int_\Omega (\mathrm{grad} v)^T \varepsilon^S (\mathrm{grad} w)\; d\Omega \end{array}\right. \end{array}$$

$$\begin{array}{rcl} -\triangle_{\mathbf{e}} \;:\; H_{\mathcal{B}}^1 & \to & (H_g^1)^* \\ \vec{b} & \mapsto & \left\{ \begin{array}{rcl} -\triangle_{\mathbf{e}}\, \vec{d} \;:\; H_g^1 & \to & \mathbb{R} \\ v & \mapsto & \int_\Omega (\mathrm{grad} w)^T \mathbf{e}(\mathcal{B}\vec{\hat{d}})\; d\Omega \end{array}\right. \end{array}$$

and $\delta_{\Gamma_e} \in (H_g^1)^*$ denotes evaluation at the loaded electrode. Inserting this into the first part ($w :\equiv 0$) of (7) corresponding to line one in (3), we get equivalence of (7) to a problem of the form

$$(L - \rho\omega^2 \mathrm{Id})\Re(\vec{\hat{d}}(\omega)) = \Re(f(\omega))\ , \quad (L - \rho\omega^2 \mathrm{Id})\Im(\vec{\hat{d}}(\omega)) = \Im(f(\omega))\ , \tag{9}$$

(and $\hat{\phi}$ being given by (8)) where $\Re(f(\omega)), \Im(f(\omega))$ are bounded linear functionals on $H_{\mathcal{B}}^1$, and the symmetric operator L induces a coercive bilinear form on $H_{\mathcal{B}}^1$, which, e.g., by Theorem 17.11 in [13], has countably many eigenvalues, that accumulate (only) at infinity. Equations (9) therefore have a unique stable solution for all but countably many values of ω — the eigenfrequencies of the system described by (3) — that do not accumulate in any finite point; this generic well-posedness result can by (8) be carried over to the whole equation (7). Analogously one sees that for any $\vec{\hat{f}}_1 \in L^2(\mathbb{R}; (H_{\mathcal{B}}^1(\Omega))^*)$, $\hat{f}_2 \in L^2(\mathbb{R}; (H_g^1(\Omega))^*)$, $\vec{\hat{g}}_0 \in L^2(\mathbb{R}; tr_{\tilde{\Gamma}}^{(1)}(H_{\mathcal{B}}^1(\Omega)))$, $\vec{\hat{g}}_1 \in L^2(\mathbb{R}; tr_{\partial\Omega\setminus\tilde{\Gamma}}^{(1)}(H_{\mathcal{B}}^1(\Omega)))$, $\hat{g}_2 \in L^2(\mathbb{R}; tr_{\Gamma_e}^{(1)}(H_g^1(\Omega)))$, $\hat{g}_3 \in L^2(\mathbb{R}; tr_{\partial\Omega\setminus(\Gamma_g\cup\Gamma_e)}^{(1)}(H_g^1(\Omega)))$, (where $tr_\Gamma^{(1)}$ is the trace operator $v \mapsto \frac{\partial v}{\partial \vec{n}}|_\Gamma$, to be understood component wise for vector valued v), for all ω different from the eigenfrequencies, there exists a unique stable weak solution $(\vec{\hat{d}}(\omega), \hat{\phi}(\omega))$ of the boundary value problem

$$\begin{array}{rcll} -\rho\omega^2\vec{\hat{d}} - \mathcal{B}^T\Big(\mathbf{c}^E\mathcal{B}\vec{\hat{d}} + \mathbf{e}^T\mathrm{grad}\hat{\phi}\Big) & = & \vec{\hat{f}}_1 & \text{in } \Omega \\ -\mathrm{div}\Big(\mathbf{e}\mathcal{B}\vec{\hat{d}} - \varepsilon^S\mathrm{grad}\hat{\phi}\Big) & = & \hat{f}_2 & \text{in } \Omega \\ \mathbf{N}^T\vec{\hat{\sigma}} & = & \vec{\hat{g}}_0 & \text{on } \tilde{\Gamma} \\ \mathbf{N}^T\vec{\hat{\sigma}} & = & \vec{\hat{g}}_1 & \text{on } \partial\Omega\setminus\tilde{\Gamma} \\ \phi & = & 0 & \text{on } \Gamma_g \\ \vec{\hat{D}}\cdot\vec{n} & = & \hat{g}_2 & \text{on } \Gamma_e \\ \vec{\hat{D}}\cdot\vec{n} & = & \hat{g}_3 & \text{on } \partial\Omega\setminus(\Gamma_g\cup\Gamma_e) \end{array}$$

i.e., of

$$\begin{aligned}
&\forall \vec{b} \in H^1_{\mathcal{B}}(\Omega) \quad w \in H^1_g(\Omega) \ : \\
&\textstyle\int_\Omega \Big(-\rho\omega^2 \vec{\hat{d}})^T \vec{b} \ + \ (\mathcal{B}\vec{\hat{d}})^T \mathbf{c}^E (\mathcal{B}\vec{b}) && + \ \ (\mathrm{grad}\hat{\phi})^T \mathbf{e}(\mathcal{B}\vec{b}) + (\mathrm{grad} w)^T \mathbf{e}(\mathcal{B}\vec{\hat{d}}) \\
& && - \ \ (\mathrm{grad}\hat{\phi})^T \varepsilon^S (\mathrm{grad} w) \Big) \ d\Omega \qquad (10) \\
&= \textstyle\int_\Omega \vec{\hat{f}}_1(\omega)^T \vec{b} \ d\Omega + \int_\Omega \hat{f}_2(\omega) w \ d\Omega && + \ \ \textstyle\int_{\tilde{\Gamma}} \vec{\hat{g}}_0(\omega)^T \vec{b} \ d\Gamma + \int_{\partial\Omega\setminus\tilde{\Gamma}} \vec{\hat{g}}_1(\omega)^T \vec{b} \ d\Gamma \\
& && + \ \ \textstyle\int_{\Gamma_e} \hat{g}_2(\omega) w \ d\Gamma + \int_{\partial\Omega\setminus(\Gamma_g \cup \Gamma_e)} \hat{g}_3(\omega) w \ d\Gamma
\end{aligned}$$

(The possible additional boundary condition on $\tilde{\Gamma} \subset \partial\Omega$ is introduced in order to eventually enable incorporation of additional boundary measurements in our inversion procedure.)

2.3 Numerical solution

In our parameter identification approach, we will repeatedly have to solve forward problems of the form (10) for several values of ω and for different right hand sides $\vec{\hat{f}}_1, \hat{f}_2, \vec{\hat{g}}_0, \vec{\hat{g}}_1, \hat{g}_2, \hat{g}_3$, which we we do by using piezoelectric finite elements (cf. [7]).

2.3.1 Space discretization with finite elements

With the ansatz

$$\begin{aligned}
\Re/\Im(\hat{d}^h_x)(x,y,z;\omega) &= \textstyle\sum_{i=1}^{n_{eq}} N^d_i(x,y,z) \Re/\Im(\mathrm{d}_{ix}) \\
\Re/\Im(\hat{d}^h_y)(x,y,z;\omega) &= \textstyle\sum_{i=1}^{n_{eq}} N^d_i(x,y,z) \Re/\Im(\mathrm{d}_{iy}) \\
\Re/\Im(\hat{d}^h_z)(x,y,z;\omega) &= \textstyle\sum_{i=1}^{n_{eq}} N^d_i(x,y,z) \Re/\Im(\mathrm{d}_{iz}) \\
\Re/\Im(\hat{\phi}^h)(x,y,z;\omega) &= \textstyle\sum_{i=1}^{n_{eq}} N^\phi_i(x,y,z) \Re/\Im(\varphi_i)
\end{aligned} \qquad (11)$$

for the real and imaginary parts of $\vec{\hat{d}^h}(\omega), \hat{\phi}^h(\omega)$, respectively, and analogously for the test functions $\vec{b}$, w, and introducing numerical damping, we arrive at a finite dimensional system of linear equations

$$\begin{pmatrix} -\omega^2 \mathbf{M}_{dd} + j\omega \mathbf{C}_{dd} + \mathbf{K}_{dd} & \mathbf{K}_{d\phi} \\ \mathbf{K}^T_{d\phi} & -\mathbf{K}_{\phi\phi} \end{pmatrix} \begin{pmatrix} \{\vec{\hat{\mathrm{d}}}\} \\ \{\hat{\varphi}\} \end{pmatrix} = \begin{pmatrix} \{\vec{\hat{F}}\} \\ \{\hat{Q}\} \end{pmatrix} ,$$

where

$$\mathbf{C}_{dd} = \alpha \mathbf{M}_{dd} + \beta \mathbf{K}_{dd}$$

with appropriate damping coefficients $\alpha, \beta \in \mathbb{R}^+$, the matrices $\mathbf{M}_{dd}$, $\mathbf{K}_{dd}$, $\mathbf{K}_{d\phi}$, $\mathbf{K}_{\phi\phi}$ consist of the element matrices

$$\begin{aligned}
m_{dd} &= \textstyle\int_\Omega \rho N^{dT} N^d \ d\Omega \quad \text{(mass matrix)} \\
k_{dd} &= \textstyle\int_\Omega (\mathcal{B}N^d)^T \mathbf{c}^E (\mathcal{B}N^d) \ d\Omega \quad \text{(stiffness matrix)} \\
k_{d\phi} &= \textstyle\int_\Omega (\mathcal{B}N^d)^T \mathbf{e} (\mathrm{grad} N^\phi) \ d\Omega \quad \text{(piezoelectric coupling matrix)} \\
k_{\phi\phi} &= \textstyle\int_\Omega (\mathrm{grad} N^\phi)^T \varepsilon^S (\mathrm{grad} N^\phi) \ d\Omega \quad \text{(permittivity matrix)}
\end{aligned}$$

and

$$\begin{aligned}
\hat{F}_{ix} &= \int_\Omega \hat{f}_{1x}(\omega) N_i^d \, d\Omega + \int_{\tilde{\Gamma}} \hat{g}_{0x}(\omega) N_i^d \, d\Gamma + \int_{\partial\Omega\setminus\tilde{\Gamma}} \hat{g}_{1x}(\omega) N_i^d \, d\Gamma \\
\hat{F}_{iy} &= \int_\Omega \hat{f}_{1y}(\omega) N_i^d \, d\Omega + \int_{\tilde{\Gamma}} \hat{g}_{0y}(\omega) N_i^d \, d\Gamma + \int_{\partial\Omega\setminus\tilde{\Gamma}} \hat{g}(\omega)_{1y} N_i^d \, d\Gamma \\
\hat{F}_{iz} &= \int_\Omega \hat{f}_{1z}(\omega) N_i^d \, d\Omega + \int_{\tilde{\Gamma}} \hat{g}_{0z}(\omega) N_i^d \, d\Gamma + \int_{\partial\Omega\setminus\tilde{\Gamma}} \hat{g}_{1z}(\omega) N_i^d \, d\Gamma \\
\hat{Q}_i &= \int_\Omega \hat{f}_2(\omega) N_i^\phi \, d\Omega + \int_{\Gamma_e} \hat{g}_2(\omega) N_i^\phi \, d\Gamma + \int_{\partial\Omega\setminus(\Gamma_g\cup\Gamma_e)} \hat{g}_3(\omega) N_i^\phi \, d\Gamma \ .
\end{aligned}$$

2.3.2 The rotational symmetric case

Since in the rotational symmetric case there holds

$$d_\theta = 0 \ , \quad \partial/\partial\theta = 0$$

we obtain for the mechanical displacements (cf. [10])

$$S_{rr} = \frac{\partial d_r}{\partial r} \tag{12}$$

$$S_{\theta\theta} = \frac{d_r}{r} \tag{13}$$

$$S_{zz} = \frac{\partial d_z}{\partial z} \tag{14}$$

$$S_{r\theta} = S_{z\theta} = 0 \tag{15}$$

$$S_{rz} = \frac{\partial d_r}{\partial z} + \frac{\partial d_z}{\partial r} \ . \tag{16}$$

Therefore the mechanical displacement-, strain-, and stress vectors change to

$$(d_r, d_z)^T \ , \quad (S_{rr}, S_{zz}, S_{rz}, S_{\theta\theta})^T \ , \quad (\sigma_{rr}, \sigma_{zz}, \sigma_{rz}, \sigma_{\theta\theta})^T \tag{17}$$

(with rotational symmetric components) and the material tensors to

$$\begin{aligned}
\breve{\mathbf{c}}^E &= \begin{pmatrix} c_{11}^E & c_{13}^E & 0 & c_{12}^E \\ c_{13}^E & c_{33}^E & 0 & c_{13}^E \\ 0 & 0 & c_{44}^E & 0 \\ c_{12}^E & c_{13}^E & 0 & c_{11}^E \end{pmatrix} \\
\breve{\mathbf{e}} &= \begin{pmatrix} 0 & 0 & e_{15} & 0 \\ e_{31} & e_{33} & 0 & e_{31} \end{pmatrix} \\
\breve{\varepsilon}^S &= \begin{pmatrix} \varepsilon_{11}^S & 0 \\ 0 & \varepsilon_{33}^S \end{pmatrix} \ .
\end{aligned}$$

With the corresponding differential operator

$$\breve{\mathcal{B}} = \begin{pmatrix} \frac{\partial}{\partial r} & 0 \\ 0 & \frac{\partial}{\partial z} \\ \frac{\partial}{\partial z} & \frac{\partial}{\partial r} \\ \frac{1}{r} & 0 \end{pmatrix}$$

the weak form of the piezoelectric equations, (6), becomes

$$
\begin{aligned}
&\forall \vec{b} \in H^1_{\breve{\mathcal{B}}\,\mathbb{C}}(D) \quad w \in H^1_{g\,\mathbb{C}}(D) \;: \\
&2\pi \int_D \Big(\rho(\tfrac{\partial^2 \vec{d}}{\partial t^2})^T \vec{b} \;+\; (\breve{\mathcal{B}}\vec{d})^T \breve{\mathbf{c}}^E (\breve{\mathcal{B}}\vec{b}) \quad + \quad (\mathrm{grad}\phi)^T \breve{\mathbf{e}}(\breve{\mathcal{B}}\vec{b}) + (\mathrm{grad} w)^T \breve{\mathbf{e}}(\breve{\mathcal{B}}\vec{d}) \\
&\qquad\qquad\qquad\qquad\qquad\qquad - \quad (\mathrm{grad}\phi)^T \breve{\varepsilon}(\mathrm{grad} w) \Big) \; r \; dr \; dz \\
&\qquad\qquad\qquad\qquad\qquad\qquad = \quad -\hat{q}^e w|_{\Gamma_e} \,,
\end{aligned}
\tag{18}
$$

where D denotes the cross sectional area of the rotational symmetric domain Ω.

Therefore, in the computationally less expensive rotational symmetric case still the whole parameter set is involved. By this fact we conjecture that it might suffice to use measurements of rotational symmetric test samples in the parameter identification procedure and hence do with two-dimensional forward computations.

3 The inverse problem

Our aim is to identify the $n_{par} = 10$ parameters

$$
\begin{aligned}
p &= (p_1, p_2, p_3, p_4, p_5, p_6, p_7, p_8, p_9, p_{10})^T \\
&= (c^E_{11}, c^E_{33}, c^E_{12}, c^E_{13}, c^E_{44}, e_{15}, e_{31}, e_{33}, \varepsilon^S_{11}, \varepsilon^S_{33})^T \;,
\end{aligned}
\tag{19}
$$

i.e., the non vanishing entries of $\mathbf{c}^E$, $\mathbf{e}$, ε^S. For this purpose, we use phase and amplitude measurements of the impedance curve

$$
Z(\omega) = \frac{U(\omega)}{I(\omega)} = \frac{\hat{\phi}|_{\Gamma_e}(\omega)}{j\omega\hat{q}^e(\omega)}
$$

for prescribed charge $\hat{q}^e = \hat{q}^e(\omega)$ at the electrode Γ_e and several (non-eigen-)frequencies ω_l, $l = 1, \ldots, n_{mp}$. Multiplication of Z with $j\omega\hat{q}^e(\omega_l)$ yields the data

$$
(\hat{y}_1, \ldots, \hat{y}_{n_{mp}}) = (\hat{\phi}|_{\Gamma_e}(\omega_1), \ldots, \hat{\phi}|_{\Gamma_e}(\omega_{n_{mp}})) \in \mathbb{C}^{n_{mp}} \;.
$$

In addition, one can, for these frequencies or part of them, measure the mechanical deformation in a boundary point, or more precisely, its mean value $\frac{1}{\tilde{A}} \int_{\tilde{\Gamma}} \hat{\vec{d}}(\omega)\, d\Gamma$ (possibly only in one space direction) over a small region $\tilde{\Gamma}$ of the boundary:

$$
(\hat{y}_{n_{mp}+1}, \ldots, \hat{y}_{n_{mp}+n^d_{mp}}) = (\frac{1}{\tilde{A}} \int_{\tilde{\Gamma}} d_{typ}^{-1} \hat{\vec{d}}(\omega_1)\; d\Gamma, \ldots, \frac{1}{\tilde{A}} \int_{\tilde{\Gamma}} d_{typ}^{-1} \hat{\vec{d}}(\omega_{n^d_{mp}})\; d\Gamma) \in \mathbb{C}^{n^d_{mp}} \;,
$$

where $\tilde{A}$ is the measure of the surface area $\tilde{\Gamma}$ and d_{typ} a typical value (or a diagonal 3 by 3 matrix of typical values in $1-$, $2-$, and $3-$ direction) for the absolute value of the displacement, whose reciprocal here serves as a weight for correctly scaling the mechanical measurements, being usually quite small as compared to the electrical ones. In sum we therefore have $n_{mp}+n^d_{mp}$ data values by measurements of electrical and partially mechanical quantities at n_{mp} different frequency points. We denote by the forward operator $\hat{\Phi}$, the application of the trace operator with respect to the $\hat{\phi}$-component, and the scaled mean evaluation operator on $\tilde{\Gamma}$ with respectb to the $\vec{\hat{d}}$-component, to the parameter-to-solution map for (7)

$$\begin{aligned} \hat{\Phi} : \mathbb{R}^{n_{par}} &\rightarrow \mathbb{R}^{n_{mp}} \\ p &\mapsto \left(\left(\hat{\phi}^l|_{\Gamma_e} \right)_{l=1,\ldots,n_{mp}}, \left(\tfrac{1}{\tilde{A}} \textstyle\int_{\tilde{\Gamma}} d_{typ}^{-1} \vec{\hat{d}}^l \; d\Gamma \right)_{l=1,\ldots,n_{mp}^d} \right) \end{aligned} , \tag{20}$$

where $(\vec{\hat{d}}^l, \hat{\phi}^l)$ solves (7) with $\omega := \omega_l$. Therewith, we can rewrite the inverse problem under consideration as a nonlinear operator equation

$$\hat{\Phi}(p) = \hat{y} \; . \tag{21}$$

This is a finite system of equations for finitely many unknowns; note however, that the evaluation of the forward operator involves an infinite dimensional problem, namely the solution of (7).

3.1 Identifiability: The one-dimensional case

An important question in this context is of course whether the searched for quantities are uniquely determined by the given data. In the special situation of only one essential space dimension, which corresponds, e.g, to a piezoelectric beam or a thickness resonator, this can be seen along the following arguments: The Fourier transformed piezoelectric equations with boundary conditions then become

$$\begin{aligned} -\rho\omega^2 \hat{d} - c^E \hat{d}_{xx} - e\hat{\phi}_{xx} &= 0 \qquad \text{in } (0,L) \\ -e\hat{d}_{xx} + \epsilon^S \hat{\phi}_{xx} &= 0 \qquad \text{in } (0,L) \\ (c^E \hat{d}_x + e\hat{\phi}_x)(0) &= 0 \\ (c^E \hat{d}_x + e\hat{\phi}_x)(L) &= 0 \\ \hat{\phi}(0) &= 0 \\ (e\hat{d}_x - \epsilon^S \hat{\phi}_x)(L) &= -\hat{q}^e \delta_L \end{aligned}$$

and therefore can be solved explicitely for all non-eigenfrequencies ω

$$\begin{aligned} \hat{d}(x) &= \frac{\hat{q}^e}{\epsilon^S} e \frac{\exp(j\lambda L) - 1}{\exp(2j\lambda L) - 1} \frac{j\lambda}{\rho\omega^2} (\exp(j\lambda x) - \exp(j\lambda(L-x))) \\ \hat{\phi}(x) &= \frac{\hat{q}^e}{\epsilon^S} \Big(\frac{e^2}{\epsilon^S} \frac{\exp(j\lambda L) - 1}{\exp(2j\lambda L) - 1} \frac{j\lambda}{\rho\omega^2} (\exp(j\lambda x) - \exp(j\lambda(L-x)) + \exp(j\lambda L) - 1) \; + H_L \Big) \; , \end{aligned}$$

where H_L denotes the Heaviside function centered at $x = L$, i.e., $H_L(x) = 0$ for $x < L$, $H_L(x) = 1$ for $x \geq L$, and $\lambda = \left(\frac{c^E + \frac{e^2}{\epsilon^S}}{\rho\omega^2} \right)^{-1/2}$. The eigenfrequencies are obviously given by $(\omega_n)_{n\in\mathbb{N}_0} = \left(\frac{\pi n}{L}\sqrt{\frac{c^E + \frac{e^2}{\epsilon^S}}{\rho}}\right)_{n\in\mathbb{N}_0}$. Therefore, the quantity

$$\hat{y}^\phi = \hat{y}^\phi(\omega) := \hat{\phi}(L) = \frac{\hat{q}^e}{\epsilon^S}\Big(\frac{e^2}{\epsilon^S}\frac{(\exp(j\lambda L)-1)^2}{\exp(2j\lambda L)-1}\frac{2j\lambda}{\rho\omega^2} + 1\Big)$$

contains information on the searched for parameters c^E, e, and ϵ^S in such a way that they can be expected to be extractable from measurements of $\hat{y}^\phi$ at three or more different values of ω. The sensitivity of these measurements to the respective coefficients shows considerable differences, as the following partial derivatives show:

$$\begin{aligned}
\frac{\partial \hat{y}^\phi}{\partial c^E} &= \frac{\hat{q}^e}{\epsilon^S}\left(-\frac{e^2}{\epsilon^S}\frac{(\exp(j\lambda L)-1)^2}{\exp(2j\lambda L)-1}\left(1+\frac{2j\lambda L\exp(j\lambda L)}{\exp(2j\lambda L)-1}\right)\frac{\lambda^3}{2\rho\omega^2}\right) , \\
\frac{\partial \hat{y}^\phi}{\partial e} &= \frac{\hat{q}^e}{\epsilon^S}\left(-\frac{e^3}{\epsilon^{S2}}\frac{(\exp(j\lambda L)-1)^2}{\exp(2j\lambda L)-1}\left(1+\frac{2j\lambda L\exp(j\lambda L)}{\exp(2j\lambda L)-1}\right)\frac{\lambda^3}{\rho\omega^2}\right. \\
&+ \left.\frac{2e}{\varepsilon^S}\frac{(\exp(j\lambda L)-1)^2}{\exp(2j\lambda L)-1}\frac{2j\lambda}{\rho\omega^2}\right) , \\
\frac{\partial \hat{y}^\phi}{\partial \epsilon^S} &= \frac{\hat{q}^e}{\epsilon^S}\left(\frac{e^4}{\epsilon^{S3}}\frac{(\exp(j\lambda L)-1)^2}{\exp(2j\lambda L)-1}\left(1+\frac{2j\lambda L\exp(j\lambda L)}{\exp(2j\lambda L)-1}\right)\frac{\lambda^3}{2\rho\omega^2}\right. \\
&- \left.\frac{2e^2}{\epsilon^{S2}}\frac{(\exp(j\lambda L)-1)^2}{\exp(2j\lambda L)-1}\frac{2j\lambda}{\rho\omega^2} - \frac{1}{\epsilon^S}\right) ;
\end{aligned}$$

inserting values of typical order of magnitude for the constants appearing in this equations ($\hat{q}^e \sim 10^{-8}C, L \sim 10^{-3}m, \rho \sim 10^3, \omega \sim 10^6, c^E \sim 10^{11}, e \sim 10, \epsilon^S \sim 10^{-8}$), we obtain

$$\frac{\partial \hat{y}^\phi}{\partial c^E} \sim 10^{-14} , \quad \frac{\partial \hat{y}^\phi}{\partial e} \sim 10^{-4} , \quad \frac{\partial \hat{y}^\phi}{\partial \epsilon^S} \sim 10^8 .$$

Even a natural scaling of the parameters ($\tilde{c^E} := 10^{-11}c^E$, $\tilde{e} := 10^{-1}\mathbf{e}$, $\tilde{\epsilon^S} := 10^8\epsilon^S$, see Subsection 3.3 below) cannot completely remove these large differences

$$\frac{\partial \hat{y}^\phi}{\partial \tilde{c^E}} \sim 10^{-3} , \quad \frac{\partial \hat{y}^\phi}{\partial \tilde{e}} \sim 10^{-3} , \quad \frac{\partial \hat{y}^\phi}{\partial \tilde{\epsilon^S}} \sim 1 .$$

This is also clear from the physical background: electrical measurements will of course contain more information on the electrical parameter than on the other ones. Taking into account additional mechanical measurements, though,

$$\hat{y}^d = \hat{y}^d(\omega) := \frac{1}{d_{typ}}\hat{d}(L) = \frac{\hat{q}^e e}{d_{typ}\epsilon^S}\frac{(\exp(j\lambda L)-1)^2}{\exp(2j\lambda L)-1}\frac{j\lambda}{\rho\omega^2}$$

with $d_{typ} \sim 10^{-12}$, and scaling as above, we get

$$\frac{\partial \hat{y}^d}{\partial \tilde{c^E}} \sim \frac{\partial \hat{y}^d}{\partial \tilde{e}} \sim \frac{\partial \hat{y}^d}{\partial \tilde{\epsilon^S}} \sim 1 .$$

So a quite nice resolution of all three material constants could be expected to be obtainable from measurements of the mechanical displacement — at the price of a practically more difficult experimental setting than with only simple impedance measurements, though.

3.2 Reconstruction by a Newton-CG algorithm

Newton's method for the iterative solution of the nonlinear equation (21) formally reads as

$$p^{k+1} = p^k + s^k \quad \text{with} \quad \hat{\Phi}'(p^k)[s^k] = \hat{y} - \hat{\Phi}(p^k) \ . \tag{22}$$

For the computation of the right hand side $\hat{y} - \hat{\Phi}(p^k)$ one therefore needs the solution $(\vec{\hat{d}}_k, \hat{\phi}_k)(\omega)$ of the Fourier transformed piezoelectric equations (7) with the tensor entries of $\mathbf{c}^E, \mathbf{e}$, and ε^S being given by the respective values in the vector p^k, for $\omega = \omega_1, \ldots \omega_{n_{mp}}$, which, as we will see below, also enters into the evaluation of $\hat{\Phi}'(p^k)$. It is computed approximately via a finite element ansatz (cf. Subsection 2.3.1); we denote the respective coefficients by $(\{\vec{\hat{\mathrm{d}}}_k^{\,l}\}, \{\hat{\varphi}_k^l\})$.

The Jakobi matrix $\hat{\Phi}'(p^k)$ is here given implicitly, via the piezoelectric equations; forming, for an increment $\underline{dp} \in \mathbb{R}^{n_{par}}$ the difference $\hat{\Phi}(p^k + \underline{dp}) - \hat{\Phi}(p^k)$ and omitting terms of higher than first order, one formally gets the derivative, i.e., the local linearization, of $\hat{\Phi}$ at p^k in direction $\underline{dp}$:

$$\hat{\Phi}'(p^k)[\underline{dp}] = \Big(\big(\underline{d\hat{\phi}}^{\,l}|_{\Gamma_e}\big)_{l=1,\ldots,n_{mp}}, \Big(\frac{1}{\tilde{A}} \int_{\tilde{\Gamma}} d_{typ}^{-1} \underline{d\vec{\hat{d}}}^{\,l} \, d\Gamma\Big)_{l=1,\ldots,n_{mp}^d} \Big) \tag{23}$$

where $(\underline{d\vec{\hat{d}}}^{\,l}, \underline{d\hat{\phi}}^{\,l})$ weakly solves (10) with

$$\begin{array}{rcl}
\vec{\hat{f}}_1 &=& \mathcal{B}^T(\underline{d\mathbf{c}^E}\mathcal{B}\vec{\hat{d}} + \underline{d\mathbf{e}}^T \mathrm{grad}\hat{\phi}) \\
\hat{f}_2 &=& \mathrm{div}(\underline{d\mathbf{e}}\mathcal{B}\vec{\hat{d}} - \underline{d\varepsilon^S}\mathrm{grad}\hat{\phi}) \\
\vec{\hat{g}}_0 &=& -\mathbf{N}^T(\underline{d\mathbf{c}^E}\mathcal{B}\vec{\hat{d}} + \underline{d\mathbf{e}}^T \mathrm{grad}\hat{\phi})|_{\tilde{\Gamma}} \\
\vec{\hat{g}}_1 &=& -\mathbf{N}^T(\underline{d\mathbf{c}^E}\mathcal{B}\vec{\hat{d}} + \underline{d\mathbf{e}}^T \mathrm{grad}\hat{\phi})|_{\partial\Omega\setminus\tilde{\Gamma}} \\
\hat{g}_2 &=& -(\underline{d\mathbf{e}}\mathcal{B}\vec{\hat{d}} - \underline{d\varepsilon^S}\mathrm{grad}\hat{\phi}) \cdot \vec{n}|_{\Gamma_e} \\
\hat{g}_3 &=& -(\underline{d\mathbf{e}}\mathcal{B}\vec{\hat{d}} - \underline{d\varepsilon^S}\mathrm{grad}\hat{\phi}) \cdot \vec{n}|_{\Gamma_g} \ ,
\end{array} \tag{24}$$

and $\underline{d\mathbf{c}^E}$, $\underline{d\mathbf{e}}$, $\underline{d\varepsilon^S}$ are the matrices formed from the respective entries in $\underline{dp}$; i.e.,

$$\begin{array}{lcl}
\forall \vec{b} \in H^1_{\mathcal{B}\,\mathbb{C}}(\Omega) \quad w \in H^1_{g\,\mathbb{C}}(\Omega) \ : & & \\
\int_\Omega \Big(-\rho\omega_l^2 (\underline{d\vec{\hat{d}}}^{\,l})^T \vec{b} \ + \ (\mathcal{B}\underline{d\vec{\hat{d}}}^{\,l})^T \mathbf{c}^E (\mathcal{B}\vec{b}) & + & (\mathrm{grad}\underline{d\hat{\phi}}^{\,l})^T \mathbf{e}(\mathcal{B}\vec{b}) + (\mathrm{grad} w)^T \mathbf{e}(\mathcal{B}\underline{d\vec{\hat{d}}}^{\,l}) \\
 & - & (\mathrm{grad}\underline{d\hat{\phi}}^{\,l})^T \varepsilon^S (\mathrm{grad} w) \Big) \ d\Omega \\
= \int_\Omega \Big(-(\mathcal{B}\vec{\hat{d}}_k^{\,l})^T \underline{d\mathbf{c}^E}(\mathcal{B}\vec{b}) - (\mathrm{grad}\hat{\phi}_k^l)^T \underline{d\mathbf{e}}(\mathcal{B}\vec{b}) & - & (\mathrm{grad} w)^T \underline{d\mathbf{e}}(\mathcal{B}\vec{\hat{d}}_k^{\,l}) \\
 & + & (\mathrm{grad}\hat{\phi}_k^l)^T \underline{d\varepsilon^S}(\mathrm{grad} w) \Big) \ d\Omega
\end{array} \tag{25}$$

and with FE space discretization one obtains for the coefficients $(\underline{d\vec{\hat{\mathrm{d}}}}^l, \underline{d\hat{\varphi}}^l)$:

$$\begin{pmatrix} -\omega_l^2\mathbf{M}_{dd} + j\omega_l\mathbf{C}_{ldd} + \mathbf{K}_{dd} & \mathbf{K}_{d\phi} \\ \mathbf{K}_{d\phi}^T & -\mathbf{K}_{\phi\phi} \end{pmatrix} \begin{pmatrix} \{\underline{d\vec{\hat{\mathrm{d}}}}^l\} \\ \{\underline{d\hat{\varphi}}^l\} \end{pmatrix} = \begin{pmatrix} \{\vec{\hat{F}}^l\} \\ \{\hat{Q}^l\} \end{pmatrix} , \tag{26}$$

(the subscript l in $\mathbf{C}_{ldd}$ is supposed to emphasize the fact that the damping matrix depends on l via the damping parameters $\alpha_l = \alpha(\omega_l)$, $\beta_l = \beta(\omega_l)$) with

$$\hat{F}^l_{ix} = -(1 + j\omega_l\beta_l)\int_\Omega \Big((\mathcal{B}\vec{\hat{d}}^l_k)^T \underline{d\mathbf{c}^E}(\mathcal{B}_x N_i^d) + (\mathrm{grad}\hat{\phi}^l_k)^T \underline{d\mathbf{e}}(\mathcal{B}_x N_i^d)\Big)\, d\Omega$$

$$\hat{Q}^l_i = \int_\Omega \Big(-(\mathrm{grad}N_i^\phi)^T \underline{d\mathbf{e}}(\mathcal{B}\vec{\hat{d}}^l_k) + (\mathrm{grad}\hat{\phi}^l_k)^T \underline{d\varepsilon^S}(\mathrm{grad}N_i^\phi)\Big)\, d\Omega$$

hence

$$\begin{pmatrix} \{\vec{\hat{F}}^l\} \\ \{\hat{Q}^l\} \end{pmatrix} \approx -\begin{pmatrix} (1 + j\omega_l\beta_l)\underline{\mathbf{dK}}_{dd} & \underline{\mathbf{dK}}_{d\phi} \\ \underline{\mathbf{dK}}_{d\phi}^T & -\underline{\mathbf{dK}}_{\phi\phi} \end{pmatrix} \begin{pmatrix} \{\vec{\hat{\mathrm{d}}}^l_k\} \\ \{\hat{\varphi}^l_k\} \end{pmatrix} .$$

The matrices $\underline{\mathbf{dK}}_{dd}$, $\underline{\mathbf{dK}}_{d\phi}$, $\underline{\mathbf{dK}}_{\phi\phi}$ are defined analogously to $\mathbf{K}_{dd}$, $\mathbf{K}_{d\phi}$, $\mathbf{K}_{\phi\phi}$ (with the material parameters p replaced by the material parameter increments $\underline{dp}$); $(\{\vec{\hat{\mathrm{d}}}_k^{\,l}\}, \{\hat{\varphi}^l_k\})$ are the coefficients known from the (approximate) computation of $\hat{\Phi}(p^k)$.

In order to obtain from this implicit representation of the Jacobi matrix a search direction s^k according to (22), i.e., the solution of a linear system with the Jacobi matrix as system matrix, we proceed iteratively, and, in order to obtain a symmetric system matrix, consider the normal equation

$$\hat{\Phi}'(p^k)^T\hat{\Phi}'(p^k)[s^k] = \hat{\Phi}'(p^k)^T(\hat{y} - \hat{\Phi}(p^k))\,. \tag{27}$$

Therefore and for the following iterative solution methods for (27) we need the transposed of $\hat{\Phi}'(p^k)$, which again we do not know explicitely as a matrix, but only applied to a direction q (—this is just what one needs for executing a CG-iteration): For arbitrary $\underline{dp} \in \mathbb{R}^{n_{par}}$, $q \in \mathbb{C}^{n_{mp}+3n^d_{mp}}$, we define $(\vec{\tilde{d}}^l, \tilde{\phi}^l)$ to be the solution of (7) with $p := p^k$, $\omega := \omega^l$, $\vec{\hat{f}}_1 := 0$, $\hat{f}_2 := 0$, $\vec{\hat{g}}_1 := 0$, $\hat{g}_2 := \frac{\overline{q}_l}{A}$, $\hat{g}_3 := 0$, and

$$\vec{\hat{g}}_0 := \begin{cases} \frac{1}{A} d_{typ}^{-1}\vec{\overline{q}}_{n_{mp}+l} & \text{for } 1 \le l \le n^d_{mp} \\ 0 & \text{for } n^d_{mp} + 1 \le l \le n_{mp} \,, \end{cases}$$

where $\overline{q}$ denotes the complex conjugate, and obtain, with the weak formulation of the piezoelectric equations for $(\vec{\tilde{d}}^l, \tilde{\phi}^l)$ and for $(\underline{d\vec{\hat{d}}}^l, \underline{d\hat{\phi}}^l)$ according to (23), respectively (see

(25)):

$$\begin{aligned}
\Re\Big((\hat\Phi'(p^k)[\underline{dp}])^T\overline{q}\Big) &= \Re\Big(\textstyle\sum_{l=1}^{n_{mp}} \underline{d\hat\phi}^l|_{\Gamma_e}\,\overline{q}_l + \sum_{l=1}^{n^d_{mp}} \int_{\tilde\Gamma}(\vec{\hat{d}}^{\,l})^T(\frac{1}{A}d_{typ}^{-1}\vec{\overline{q}}_{n_{mp}+l})\ d\Gamma\Big)\\
&= \Re\Big(\textstyle\sum_{l=1}^{n_{mp}} \int_\Omega\Big(-(\mathcal{B}\vec{\hat{d}}^{\,l}_k)^T\underline{d\mathbf{c}^E}(\mathcal{B}\vec{\tilde{d}}^{\,l}) - (\mathrm{grad}\hat\phi^l_k)^T\underline{d\mathbf{e}}(\mathcal{B}\vec{\tilde{d}}^{\,l})\\
&\qquad -(\mathrm{grad}\tilde\phi^l)^T\underline{d\mathbf{e}}(\mathcal{B}\vec{\hat{d}}^{\,l}_k) + (\mathrm{grad}\hat\phi^l_k)^T\underline{d\varepsilon^S}(\mathrm{grad}\tilde\phi^l)\Big)\ d\Omega\Big)\\
&\approx \Re\Big(\textstyle\sum_{l=1}^{n_{mp}} \int_\Omega\Big(-(1+j\omega_l\beta_l)(\mathcal{B}\vec{\hat{d}}^{\,lh}_k)^T\underline{d\mathbf{c}^E}(\mathcal{B}\vec{\tilde{d}}^{\,lh}) - (\mathrm{grad}\hat\phi^{lh}_k)^T\underline{d\mathbf{e}}(\mathcal{B}\vec{\tilde{d}}^{\,lh})\\
&\qquad -(\mathrm{grad}\tilde\phi^{lh})^T\underline{d\mathbf{e}}(\mathcal{B}\vec{\hat{d}}^{\,lh}_k) + (\mathrm{grad}\hat\phi^{lh}_k)^T\underline{d\varepsilon^S}(\mathrm{grad}\tilde\phi^{lh})\Big)\ d\Omega\Big)\ .
\end{aligned}$$

Introducing the simple matrices

$$P^{(z,s)}_{Z\times S}\in\mathbb{R}^S_Z\ ,\quad (P^{(z,s)}_{Z\times S})_{ij} = \begin{cases} 1 & \text{falls } i=z \text{ und } j=s\\ 0 & \text{otherwise}\end{cases}$$

and assembling them to

$$\begin{array}{lcl@{\qquad}lcl}
\mathbf{P}^1 &:=& P^{(1,1)}_{6\times6}+P^{(2,2)}_{6\times6}+\frac12 P^{(4,4)}_{6\times6} & \mathbf{P}^6 &:=& P^{(1,6)}_{3\times6}+P^{(2,5)}_{3\times6}\\
\mathbf{P}^2 &:=& P^{(3,3)}_{6\times6} & \mathbf{P}^7 &:=& P^{(3,1)}_{3\times6}+P^{(3,2)}_{3\times6}\\
\mathbf{P}^3 &:=& P^{(1,2)}_{6\times6}+P^{(2,1)}_{6\times6}-\frac12 P^{(4,4)}_{6\times6} & \mathbf{P}^8 &:=& P^{(3,3)}_{3\times6}\\
\mathbf{P}^4 &:=& P^{(1,3)}_{6\times6}+P^{(3,1)}_{6\times6}+P^{(2,3)}_{6\times6}+P^{(3,2)}_{6\times6} & \mathbf{P}^9 &:=& P^{(1,1)}_{3\times3}+P^{(2,2)}_{3\times3}\\
\mathbf{P}^5 &:=& P^{(5,5)}_{6\times6}+P^{(6,6)}_{6\times6} & \mathbf{P}^{10} &:=& P^{(3,3)}_{3\times3}\ ,
\end{array}$$

representing the sparsity pattern of the material tensors and corresponding to the respective coefficients, we can write

$$\begin{aligned}
\underline{d\mathbf{c}^E} &= \underline{dc^E_{11}}\mathbf{P}^1+\underline{dc^E_{33}}\mathbf{P}^2+\underline{dc^E_{12}}\mathbf{P}^3+\underline{dc^E_{13}}\mathbf{P}^4+\underline{dc^E_{44}}\mathbf{P}^5\\
\underline{d\mathbf{e}} &= \underline{de_{15}}\mathbf{P}^6+\underline{de_{31}}\mathbf{P}^7+\underline{de_{33}}\mathbf{P}^8\\
\underline{d\varepsilon^S} &= \underline{d\varepsilon_{11}}\mathbf{P}^9+\underline{d\varepsilon_{33}}\mathbf{P}^{10}
\end{aligned}$$

and therefore, with stiffness-, coupling-, and permittivity type matrices $\mathbf{K}^i_{dd}$, $\mathbf{K}^i_{d\phi}$, $\mathbf{K}^i_{\phi\phi}$, $i=1,\ldots,10$, formed from the element matrices

$$\begin{aligned}
k^i_{dd} &:= \textstyle\int_\Omega(\mathcal{B}N^d)^T\mathbf{P}^i(\mathcal{B}N^d)\ d\Omega\ ,\\
k^i_{d\phi} &:= \textstyle\int_\Omega(\mathcal{B}N^d)^T\mathbf{P}^i(\mathrm{grad}N^\phi)\ d\Omega\ ,\\
k^i_{\phi\phi} &:= \textstyle\int_\Omega(\mathrm{grad}N^\phi)^T\mathbf{P}^i(\mathrm{grad}N^\phi)\ d\Omega
\end{aligned}$$

we get

$$\begin{aligned}
\Big(\hat\Phi'(p^k)^T[q]\Big)_i &= -\textstyle\sum_{l=1}^{n_{mp}}\Re\Big(\int_\Omega(\mathcal{B}\vec{\hat{d}}^{\,l}_k)^T\mathbf{P}^i(\mathcal{B}\vec{\tilde{d}}^{\,l})\ d\Omega\Big)\\
&\approx -\textstyle\sum_{l=1}^{n_{mp}}\Re\Big((1+j\omega_l\beta_l)(\vec{\hat{\mathrm{d}}}^{\,l}_k)^T\mathbf{K}^i_{dd}(\vec{\tilde{\mathrm{d}}}^{\,l})\Big)\ ,\quad i=1,\ldots 5\\
\Big(\hat\Phi'(p^k)^T[q]\Big)_i &= -\textstyle\sum_{l=1}^{n_{mp}}\Re\Big(\int_\Omega\Big((\mathrm{grad}\hat\phi^l_k)^T\mathbf{P}^i(\mathcal{B}\vec{\tilde{d}}^{\,l})+(\mathrm{grad}\tilde\phi^l)^T\mathbf{P}^i(\mathcal{B}\vec{\hat{d}}^{\,l}_k)\Big)d\Omega\Big)\\
&\approx -\textstyle\sum_{l=1}^{n_{mp}}\Re\Big((\hat\varphi^l_k)^T\mathbf{K}^i_{d\phi}(\vec{\tilde{\mathrm{d}}}^{\,l})+(\tilde\varphi^l)^T\mathbf{K}^i_{d\phi}(\vec{\hat{\mathrm{d}}}_k)\Big)\ ,\quad i=6,7,8\\
\Big(\hat\Phi'(p^k)^T[q]\Big)_i &= -\textstyle\sum_{l=1}^{n_{mp}}\Re\Big(\int_\Omega(\mathrm{grad}\hat\phi^l_k)^T\mathbf{P}^i(\mathrm{grad}\tilde\phi^l)\ d\Omega\Big)\\
&\approx -\textstyle\sum_{l=1}^{n_{mp}}\Re\Big((\hat\varphi^l_k)^T\mathbf{K}^i_{\phi\phi}(\tilde\varphi^l)\Big)\ ,\quad i=9,10
\end{aligned}\tag{28}$$

Therewith we can implement a CG iteration for the computation of the Newton step from (27):

Algorithm 1. (CONJUGATE GRADIENT ITERATION)

CHOOSE $s^k_{(0)}$
$res_{(0)} = \hat{y} - \hat{\Phi}(p^k) - \hat{\Phi}'(p^k)[s^k_{(0)}]$,
$bas_{(1)} = res^{NE}_{(0)} = \hat{\Phi}'(p^k)^T[res_{(0)}]$,
FOR $m = 1, 2, \ldots$ (UNTIL CONVERGENCE):

$$\begin{aligned}
&\overline{bas}_{(m)} = \hat{\Phi}'(p^k)[bas_{(m)}]\\
&\alpha_{(m)} = \tfrac{||res^{NE}_{(m-1)}||^2}{||\overline{bas}_{(m)}||^2}\\
&s^k_{(m)} = s^k_{(m-1)} + \alpha_{(m)} bas_{(m)}\\
&res_{(m)} = res_{(m-1)} - \alpha_{(m)} \overline{bas}_{(m)}\\
&res^{NE}_{(m)} = \hat{\Phi}'(p^k)^T[res_{(m)}]\\
&\beta_{(m)} = \tfrac{||res^{NE}_{(m)}||^2}{||res^{NE}_{(m-1)}||^2}\\
&bas_{(m+1)} = res^{NE}_{(m)} + \beta_{(m)} bas_{(m)}
\end{aligned}$$

We set $s^k_{(0)} := 0$ and stop the iteration, as soon as the norm of the linear residual is significantly below the one of the overall residual:

$$||res_{(m)}|| = ||\hat{y} - \hat{\Phi}(p^k) - \hat{\Phi}'(p^k)[s^k_{(m)})]|| \leq \eta_k ||\hat{y} - \hat{\Phi}(p^k)||$$

with $\eta_k \leq \bar{\eta} < 1$, i.e., we carry out an inexact Newton method, that reduces effort by taking into account the fact that at the beginning of the Newton iteration — "far away" from the solution — it suffices to use a rough approximation of the Newton step as a search direction, in order to obtain the desired convergence speed. To get locally super linear convergence, η_k should go to zero as $k \to \infty$; $\eta_k \sim \|\hat{\Phi}(p_k)\|$ gives local quadratic convergence.

As a stopping criterion for the outer iteration, i.e., Newton's method, we use a discrepancy type principle: here the iteration is stopped as soon as it falls below the data noise level δ, i.e.,

$$\|\hat{y} - \hat{\Phi}(p^k)\| \leq \tilde{\tau}\delta$$

with an a priori fixed constant $\tilde{\tau} > 1$.

3.3 Further aspects in measurement technique and computational implementation

Measurements of c^E_{33}

One should take care of the fact that still some of the searched for parameters might be accessible to direct measurements. E.g., the parameter c^E_{33} can be measured by the following experimental setup as shown in Fig. 1. For the generation as well as signal conditioning of the receiving piezoelectric signal the measurement system RAM 10000 is used. By measuring the phase change of the first (buffer rod - sample interface) and second

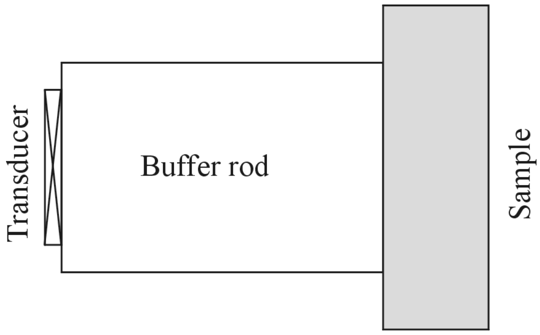

Figure 1: Experimental setup

(top of sample) echo at time zero and time t, the transit time t_{transit} is computed by [11]

$$t_{\text{transit}} = \frac{(\varphi_{r2}(t) - \varphi_{r1}(t)) - (\varphi_{r2}(0) - \varphi_{r1}(0))}{2\omega} \tag{29}$$

with $\varphi_{ri}(t)$ the phase of the i^{th} echo signal at time t, $\varphi_{ri}(0)$ the phase at time zero and ω the frequency of the signals. Therewith, the longitudinal velocity c_{L} of the wave in the sample is computed with its thickness d by

$$c_{\text{L}} = \frac{d}{t_{\text{transit}}} \,. \tag{30}$$

By this information and the knowledge of the density ρ of the sample the parameter c_{33}^E is given by [6]

$$c_{33}^E = \rho c_{\text{L}}^2 \,. \tag{31}$$

Identification of a subset of the parameters

If we want to identify only a part of the material parameters, and assume the rest of them to be known, then this means that (21) is replaced by

$$\acute{\Phi}(\acute{p}) = \hat{y} \ , \tag{32}$$

where $\acute{p} := (\acute{p}_1, \ldots, \acute{p}_{\acute{n}_{par}})$ with $\acute{n}_{par} \leq n_{par}$ the (now shorter) vector of searched for parameters. This modified problem and its solution can in an obvious way, but also formally correctly, be derived from the original situation of identifying all coefficients, by introducing an affine mapping

$$\acute{p} \in \mathbb{R}^{\acute{n}_{par}} \mapsto A\acute{p} + b \in \mathbb{R}^{n_{par}}$$

that maps such a shorter parameter into a full parameter set by placing the unknowns contained in $\acute{p}$ to the corresponding positions according to (19) and filling up the remaining positions in p with the known parameter values. The matrix A with n_{par} lines and $\acute{n}_{par}$ columns, therefore consists of the $\acute{n}_{par}$-dimensional unit matrix with inserted zero lines; the vector $b \in \mathbb{R}_{n_{par}}$ contains the $n_{par} - \acute{n}_{par}$ known parameter values at the corresponding places, and zeros, else. So $\acute{\Phi}$ in (32) is given by

$$\acute{\Phi}(\acute{p}) = \hat{\Phi}(A\acute{p} + b)$$

with $\hat{\Phi}$ as in (20). A Newton-CG algorithm can, analogously to the previous section, be used for the iterative solution of (32); here $\acute{\Phi}'(\acute{p}^k)$ and its transposed can be easily computed by the chain rule: $\acute{\Phi}'(\acute{p}^k) = \hat{\Phi}'(A\acute{p}^k + b)A$, $\acute{\Phi}'(\acute{p}^k)^T = A^T\hat{\Phi}'(A\acute{p}^k + b)^T$. The fact that in the situation of less searched for parameters one will also use less measurements, does not disturb our formalism, since n_{mp} in the previous section can be an arbitrary positive integer.

Damping parameters

As mentioned in Subsection 2.3, we consider Rayleigh damping, i.e., we add to the left hand side in (7) the two terms $\int_\Omega j\omega\rho\alpha\hat{\vec{d}}^T\vec{b}\,d\Omega$ and $\int_\Omega j\omega\beta(\mathcal{B}\hat{\vec{d}})^T\mathbf{c}^E(\mathcal{B}\vec{b})\,d\Omega$ with $\alpha, \beta > 0$. These parameters depend on the frequency, (the typical order of magnitude in the range of interest of $1-2$ MHz being $\alpha \sim 10^4$, $\beta \sim 10^{-9}$,) and can be measured directly by using the same measurement setup as used for the determination of the longitudinal velocity c_L (see Fig. 1). By selecting the first and second echo signal the absolute attenuation γ is computed via

$$\gamma = 20\log\frac{G_1A_1}{G_2A_2}\,, \tag{33}$$

where G_1, G_2 denote the gain settings and A_1, A_2 the amplitudes of the first and second echo. Supposing a viscous damping, the logarithmic decrement D defines the decrease of amplitude between two subsequent maxima u_1 and u_2 [3]

$$D = \ln\frac{u_1}{u_2} = \frac{\ln 10}{20\,\mathrm{dB}}\gamma_0 \tag{34}$$

with γ_0 the absolute damping related to the wavelength λ

$$\gamma_0 = \gamma\,\frac{\omega\lambda}{2d\omega} = \gamma\,\frac{\pi c_\mathrm{L}}{d\omega}\,. \tag{35}$$

The relation between D and the damping parameter ξ of a viscous damped oscillation is then

$$\xi = \sqrt{\frac{D^2}{D^2 + 4\pi^2}}\,. \tag{36}$$

Based on the physical assumption that the damping consists of a mass proportional and a stiffness proportional term

$$\xi(\omega) = \frac{1}{2}\left(\frac{\alpha}{\omega} + \beta\omega\right) \ , \tag{37}$$

where the parameters α and β show relatively small changes in dependence of ω, we can find $\alpha = \alpha(\omega) \approx \alpha(\omega+\delta\omega) \approx \alpha(\omega-\delta\omega)$, $\beta = \beta(\omega) \approx \beta(\omega+\delta\omega) \approx \beta(\omega-\delta\omega)$, where $\delta\omega$ is s small frequency increment, from inserting values of ξ corresponding to measurements at the two frequency points $\omega-\delta\omega$, $\omega+\delta\omega$ into (37), and resolving for α and β.

Scaling

Since the values of the searched for parameters are of quite different order of magnitude ($\mathbf{c}^E \sim 10^{11}$, $\mathbf{e} \sim 10$, $\varepsilon^S \sim 10^{-8}$,) a proper scaling of the parameter space is necessary, i.e., we apply Newton-CG to $\Psi(\xi) = \hat{y}$ with $\xi := \mathrm{Scal} \cdot p$, $\Psi(\xi) := \hat{\Phi}(\mathrm{Scal}^{-1} \cdot \xi)$, where, e.g., $\mathrm{Scal} := \mathrm{diag}(10^{-11}, \dots, 10^{-11}, 0.1, 0.1, 0.1, 10^8, 10^8)$. Newton's method is known to be invariant with respect to scaling; for the inner iteration (CG) there are a few changes, namely

$$\begin{aligned}
\alpha_{(m)} &= \frac{||\mathrm{Scal}\cdot res^{NE}_{(m-1)}||^2}{||\overline{bas}_{(m)}||^2} \\
res^{NE}_{(m)} &= \mathrm{Scal}^{-2}\hat{\Phi}'(p^k)^T[res_{(m)}] \\
\beta_{(m)} &= \frac{||\mathrm{Scal}\cdot res^{NE}_{(m)}||^2}{||\mathrm{Scal}\cdot res^{NE}_{(m-1)}||^2} \ .
\end{aligned}$$

Linesearch

Often we can assume that we have quite good starting values for our iterative identification process described in Subsection 3.2, using the estimates from the conventional experimental reconstruction methods as described in the introduction, or the material parameters of similar known piezoelectric media. However, if this is not the case or, as it has turned out in our computations, some of the parameters are extremely sensitive to perturbations in the starting values, the implementation of an additional lineseach strategy seems to be advisable. We here use a simple variant of the linesearch algorithm INB as proposed and analyzed in [2], that is based on comparison of predicted and actual reduction of the residual and adapted to inexact Newton methods.

Algorithm 2. (INB, INEXACT NEWTON BACKTRACKING METHOD)

CHOOSE p_0, $\eta_{\max} \in [0,1)$, $t \in (0,1)$, AND $0 < \theta_{\min} < \theta_{\max} < 1$
FOR $k = 0, 1, 2, \dots$ (UNTIL CONVERGENCE):
  CHOOSE $\eta_k \in [0, \eta_{\max}]$
  AND s^k SUCH THAT $\|\hat{y} - \hat{\Phi}(p^k) - \hat{\Phi}'(p^k)[s^k]\| \leq \eta_k \|\hat{y} - \hat{\Phi}(p^k)\|$
  WHILE $\|\hat{y} - \hat{\Phi}(p^k + s^k)\| > (1 - t(1-\eta_k))\|\hat{y} - \hat{\Phi}(p^k)\|$:
    CHOOSE $\theta \in [\theta_{\min}, \theta_{\max}]$
    SET $s^k := \theta s^k$

AND $\eta_k := 1 - \theta(1-\eta_k)$
SET $p^{k+1} := p^k + s^k$.

Following reference [9], that describes an implementation of this algorithm, we choose the steering parameters as follows:

$$\theta_{\min} := 0.1 \ , \quad \theta_{\max} := 0.5 \ , \tag{38}$$

θ minimizes a quadratic polynomial, interpolating the real function $\theta \mapsto \|\hat{y} - \hat{\Phi}(p^k + \theta s^k)\|^2$,

$$t = 10^{-4} \tag{39}$$

$$\eta_{\max} := 0.9 \tag{40}$$

$$\begin{aligned} &\eta_0 \in [0,1) \\ &\text{fix } \gamma \in [0,1] \text{ and } \alpha \in (1,2] \\ &\eta_k := \gamma \left(\frac{\|\hat{y} - \hat{\Phi}(p^k)\|}{\|\hat{y} - \hat{\Phi}(p^{k-1})\|} \right)^{\alpha} \\ &\text{if } \gamma \eta_{k-1}^{\alpha} > 0.1 \ , \ \text{set } \eta_k := \max\{\eta_k, \gamma\eta_{k-1}^{\alpha}\} \end{aligned} \tag{41}$$

and

$$\begin{aligned} &\text{if } \eta_k > \eta_{\max} \ , \ \text{set } \eta_k := \eta_{\max} \\ &\text{if } \eta_k \le \frac{2\tilde{\tau}\delta}{\|\hat{y} - \hat{\Phi}(p^k)\|} \ , \ \text{set } \eta_k := \frac{0.8\tilde{\tau}\delta}{\|\hat{y} - \hat{\Phi}(p^k)\|} \end{aligned} \tag{42}$$

4 Numerical results

The developed Newton-CG algorithm has been tested for the automatic reconstruction of the essential material parameters of a thickness resonator (see Fig. 2) with the relationship 1 : 40 between thickness and diameter, made of PZT5A, from impedance measurements alone. Therewith, it is necessary to compute the three material parameters c_{33}^E, e_{33} and ε_{33}^S

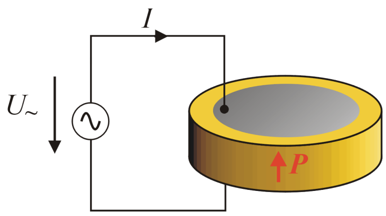

Figure 2: Thickness resonator

simultaneously.

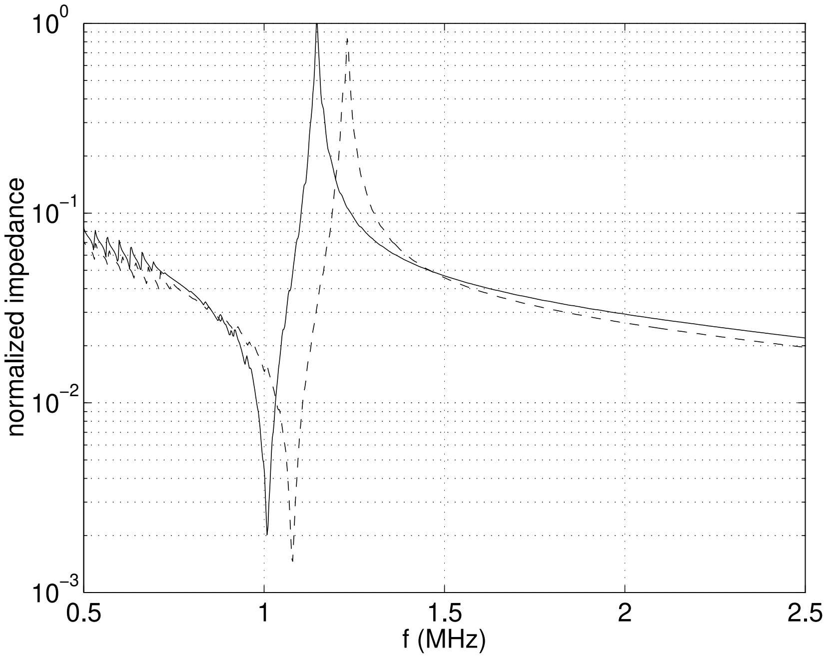

Figure 3: Normalized amplitude of electrical impedance for starting (dashed line) and correct (solid line) material parameters

Each of these material parameters has been changed by an amount of 15 % to what we here regarded as the "inexact" material parameters, and for comparison the amplitude as well as phase of the impedance curve have been computed once for the correct and once for the modified parameters (see Fig. 3 and 4). As it can be recognized from these two pictures, the change in the electrical impedance is large and the inexact parameters would therefore be too inaccurate for numerical simulations.

The impedance curve, obtained from the correct material parameters, served as the "measured" one. Therewith, the amplitude and the phase at different frequency points were used as the input data of the proposed Newton-CG algorithm, which was started at the inexact parameter values. Fig. 5 displays the relative error development of all three material parameters. It can be seen, that after 12 Newton iterations the correct values of c_{33}^E, e_{33} and ε_{33}^S are achieved. The computation has been performed on an SGI Octane R12000 and the elapsed CPU time for the total computer run was 15 seconds.
To obtain this result, it was essential to use the proposed scaling in the parameter space and the linesearch algorithm INB as described in the previous section.

5 Conclusions and Remarks

In this paper we present a new approach for the identification of piezoelectric material parameters from impedance (and optionally mechanical displacement) measurements. As

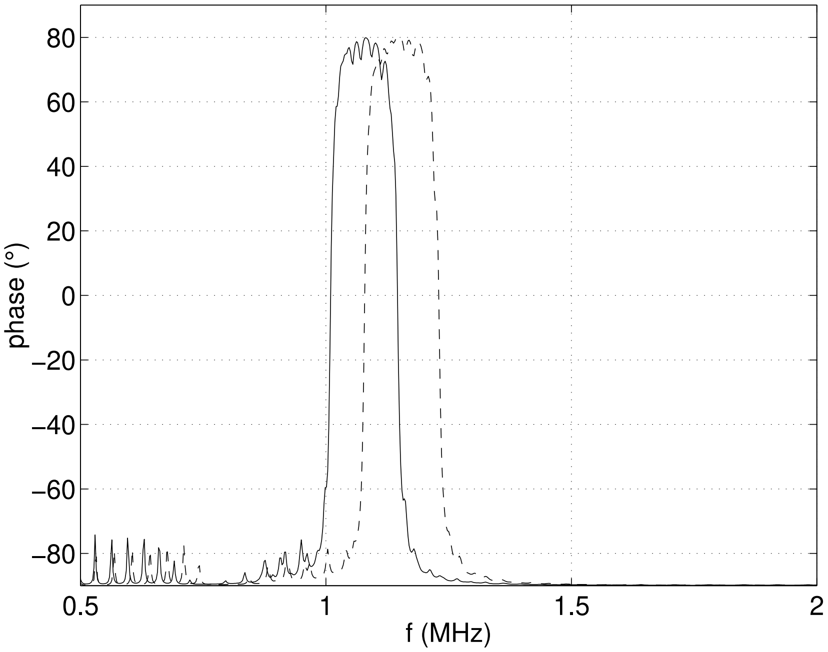

Figure 4: Phase of electrical impedance for starting (dashed line) and correct (solid line) material parameters

opposed to state-of-art estimation techniques, our method is based on forward simulations of the full two or three dimensional piezo differential equations, incorporated into an iterative inversion scheme consisting of an inexact Newton method with a conjugate gradient iteration. We address the question of well-posedness of the forward problem, and of identifiability of the parameters from the given measurements. Moreover, several measurement technical and algorithmical aspects are discussed, and the method is numerically tested on synthetic data for a thickness resonator showing considerable advantages over conventional parameter estimators.

Further work will be concerned with designing a set of simple test samples such that the full parameter set can be reconstructed; moreover in order to take into account also production caused deviations in the material properties we want to identify all essential parameters for more complicated concrete transducers from impedance and mechanical measurements. Both these tasks can be expected to be tractable by the existing computational tools.

In a next step we will consider dependence of the parameters on the stress and the electric field in the then nonlinear piezo differential equations, as it turns up in the situation of large deformations and/or currents (think e.g., of high intensity ultrasound generation). Since in this case we have to reconstruct not only real (or complex) numbers but functions of one or more variables, the question of identifiability will have to be answered beforehand, i.e., we will have to investigate whether the available measurements provide sufficient in-

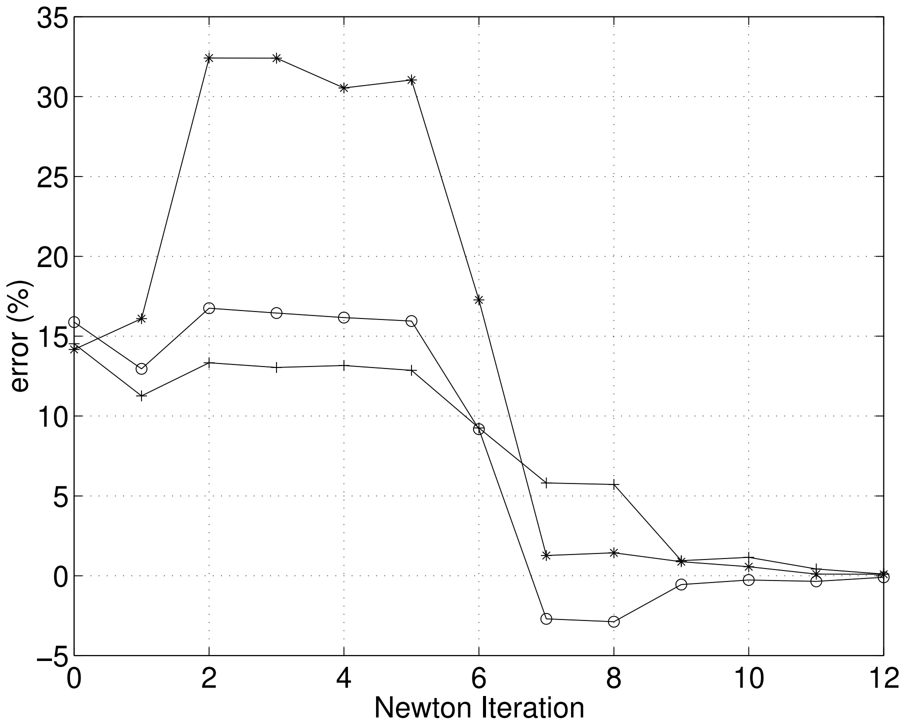

Figure 5: Relative error development for the reconstruction of c_{33}^E (marked by $+$), e_{33} (marked by o) and ε_{33}^S (marked by $*$)

formation for the reconstruction of the searched for quantities, and, if this is not the case, introduce and carry out additional measurements in order to guarantee unique identifiability. In addition to the fact that the forward computations become more demanding in the nonlinear situation, the inverse problem of parameter identification will be ill-posed in the sense of unstable dependence on the data, whence we will have to incorporate regularization (cf., e.g., [1]). This can, e.g., be done by proceeding in principle like in the constant coefficient case, namely applying a Newton-CG iteration, combined with appropriate stopping rules for the inner and outer iteration loops, respectively, that are supposed to find the optimal balance between the approximation error and the propagated data noise.

References

[1] H.W. Engl, M. Hanke, A. Neubauer, *Regularization of Inverse Problems*, Kluwer, Dordrecht, 1996.

[2] S.C. Eisenstat, H.F. Walker, *Globally convergent inexact Newton methods*, SIAM J. Optim., 4 (1994, 393-422.

[3] W. Friedrich *Analyse von Piezoelektrischen Ultraschall-Arrayantennen in Wechselwirkung mit fluiden Medien*, Dissertation, Bochum, 1992.

[4] IEEE-UFFC, *IEEE Standard on Piezoelectricity*, 1985.

[5] H. Jaffe, D.A. Belincourt, *Piezoelectric transducer materials*, Proceedings of the IEEE 53 (1965), 1372-1386.

[6] G.S. Kino *Acoustic Waves: Devices, Imaging, and Analog Signal Processing*, Prentice-Hall. Inc., 1987.

[7] R. Lerch, *Simulation of Piezoelectric devices by two- and three- dimensional finite elements*, IEEE Transactions on Ultrasonics, Ferroelectrics, and Frequency control 37 (1990), 232-247.

[8] R. Lerch, *Verbesserung des Verfahrens zur Bestimmung der elektroelastischen Tensoren von piezokeramischen Materialien*, technical report, University of Linz, 1996.

[9] M. Pernice, H.F. Walker, *NITSOL: A Newton iterative solver for nonlinear systems*, SIAM J. Sci. Comput. 19 (1998), 302-318.

[10] Parkus, *Technische Mechanik*, Springer-Verlag, 1986.

[11] RITEC Inc., *Advanced Measurement System Operation Manual*, 1996.

[12] Siemens *Vibrit. Piezokeramik von Siemens*, Siemens AG, Redwitz.

[13] J. Wloka, *Partielle Differentialgleichungen*, Teubner, Stuttgart, 1982.